Understanding Boron Chemistry as the Surface Modification and Electrolyte Additive for Co-free Lithium-Rich Layered Oxide

Na Ri Park[1], Minghao Zhang[1,*], Bing Han[1], Bryant Dang[1], Weikang Li[1], Kun Qian[1], HongNam Nguyen[2], Shinichi Kumakura[2], Wendy Zhou[2], and Ying Shirley Meng[1, 3,*]

[1] *Department of NanoEngineering, University of California San Diego, La Jolla, CA 92093, USA*

[2] *Umicore, Entrance 1A RBM-PCCa, Watertorenstreet 37A, Olen, 2250, Belgium*

[3] *Pritzker School of Molecular Engineering, The University of Chicago, Chicago, IL 60637, USA*

Email: miz016@eng.ucsd.edu; shirleymeng@uchicago.edu

Abstract

Lithium-rich layered oxide (LRLO) stands out as a highly promising cathode material for the next generation of Li-ion batteries, owing to its exceptional lithium storage capacity. The absence of cobalt in LRLO's composition provides an additional advantage, enabling cost-effective production and thereby improving the feasibility of large-scale manufacturing. Despite these promising attributes, LRLO has encountered challenges related to poor cycling performance and severe voltage decay, impeding its practical application. In addressing these challenges, we employ a surface modification technique involving lithium borate (LBO)

through a dry coating method. The LBO-coated LRLO exhibits a uniform surface layer with a thickness of 15 nm. Furthermore, the performance of LBO-coated LRLO in a full cell is synergistically enhanced when combined with lithium bis(oxalato)borate (LiBOB) as an electrolyte additive. A discharge capacity retention of 82% is achieved after 400 cycles at room temperature. These substantial improvements are attributed to the continual reaction between boron species on the LRLO cathode surface and PF_6^- anions in the electrolyte. This reaction generates BF_4^- and suppresses HF acid formation during the high voltage charging process, demonstrating LRLO's potential for practical implementation.

Introduction

Li-ion batteries have been extensively investigated, particularly in the context of emerging applications such as electric vehicles (EVs), hybrid electric vehicles (HEVs), portable electronic devices, and energy storage systems. These applications require advanced lithium storage capacity, increased energy density (calculated as the product of specific capacity and average operating voltage), and prolonged battery cycle performance [1]. The ongoing progress in battery systems that meet these demanding requirements underscores the critical nature of cathode development, as the cathode is a key component in Li-ion batteries. In pursuit of this objective, LRLO emerges as a promising candidate for the cathode material [2]. A notable characteristic of the LRLO cathode material is the remarkable reversible capacity of 250 mAh/g within the voltage range of 2.0 to 4.7 V [3]. Importantly, the incorporation of cost-effective manganese as a substitute for the more expensive nickel and cobalt elements holds significant potential for reducing production costs [4].

The practical implementation of LRLO is hindered by capacity degradation and voltage decay observed in full cell performance, particularly at high voltages [5]. The elevation of the

operating voltage introduces undesirable outcomes, including cathode-electrolyte interfacial reactions, structural transformations, and the formation of lower-voltage redox couples [6]. These effects are posited to initiate at the cathode surface, progressively extending into the bulk over successive cycles [7]. It is acknowledged that the distinctive characteristic of LRLO is oxygen redox activation at high voltages (>4.5 V versus Li/Li^+) [8]. This activation gives rise to a cascade of issues during cycling: irreversible oxygen loss, the generation of oxygen vacancies on the surface, migration and dissolution of transition metals, and the redeposition of transition metals on both cathode and anode surfaces [9].

Extensive efforts have been directed toward mitigating capacity and voltage decay in LRLO through the implementation of cathode surface modifications [10]. This strategic focus arises from the recognition that all pertinent parasitic reactions manifest most actively at the cathode's surface. Diverse methodologies for modifying the surface of LRLO cathode material have been explored, including the wet coating method [11], atomic layer deposition (ALD) [12], and solution-processable method [13]. A sol-gel based wet coating method, involving the dissolution of $Al(NO_3)_3 \cdot 9H_2O$ and NH_4F in deionized water, was employed by Zhao et al. to establish stable integrated layered-spinel structures [11]. However, the wet coating method utilizing water requires additional chemical infrastructure, including explosion-proof facilities, complicating the commercialization process. Furthermore, the rate capability reported needs to be verified in full cells. X. Zhang et al. utilized the spray pyrolysis process, employing the ALD method, to coat the cathode surface with a very thin layer of Al_2O_3, approximately 2-3 nm in thickness. This coating significantly improved the initial Coulombic efficiency and cycling performance of the coin half-cell. However, it also led to an approximately 10% decrease in the initial discharge capacity compared to the uncoated cathode, indicating a lithium inventory loss through the coating [12]. S. Kim et al. coated the surface of LRLO with polydopamine (PDA), an oxygen radical scavenger, to form

a chemically protective layer, demonstrating an 82% retention in coin half-cell cycling after 200 cycles at room temperature. The use of a self-polymerizing solution impregnation technique for coating poses challenges for mass production due to the necessity of filtering powder during the coating process and subsequent washing with ethanol and deionized water [13].

Another approach employed for cathode surface treatment is the dry coating method, wherein a solid phase identical to that of the cathode material is utilized, thereby eliminating any heterogeneity between the cathode and the coating material [14]. Notably, the mass production of dry coating is streamlined, involving the straightforward addition of the coating material during the mixing process, without necessitating supplementary infrastructure for commercialization. Consequently, the present study endeavors to advance the properties of the cathode toward commercial viability through the implementation of the dry coating method for surface treatment.

Along with determining the surface modification method, the choice of an appropriate surface modification material is pivotal in achieving performance improvements. A large number of compounds have been investigated, such as fluorides [15], phosphates [16], and oxides [11, 12]. Fluorides involve the partial doping of F^- into the surface lattice of the oxide, enhancing surface conductivity. However, fluorides have traditionally been utilized in high-Ni cathode materials where excess lithium is prevalent on the surface [17]. Phosphates are also known for their ease of reaction with excess lithium and the absorption of water in the electrolyte [18]. While Li_3PO_4 is preferred due to its ionic conductivity, in the high working voltage range of LRLO, it can readily react with free protons. This reaction leads to the formation of H_3PO_4, consequently inducing a shift in the cell environment towards a deleterious acidic state. Oxides are electrochemically stable materials [19], generally

exhibiting low electrical conductivity, thereby minimizing parasitic reactions of the cathode materials with the electrolyte. Moreover, the versatility in designing various oxides provides flexibility to tailor properties in accordance with specific requirements. Various oxides, such as Li_2ZrO_3 [20], Li_3PO_4 [21], AlF_3 [15], $MgPO_4$ [22], CeO_2 [23], and Al_2O_3 [24] have been applied for the surface modification of LRLO to improve cycling stability. Nevertheless, these published results encounter challenges in mitigating the initial irreversible capacity loss, and the application of such inactive oxides as coatings may potentially diminish the reversible capacity.

In this work, we applied surface modification to Co-free LRLO ($Li_{1.222}Ni_{0.349}Mn_{0.651}O_2$) using a dry coating process with LBO based on an organic nano-sized boron precursor. LBO coating materials are introduced as: (1) it protects the surface lattice oxygen of LRLO, reducing the exacerbated generation of H_2O and free protons at high voltage; (2) it also reacts with PF_6^- to form thermodynamically stable BF_4^-, mitigating the generation of HF acid in the electrolyte. The quality of surface modification was assessed through electron energy loss spectroscopy (EELS) obtained via scanning transmission electron microscopy (STEM). Our analysis revealed the 15 nm uniform distribution of LBO coating on the LRLO surface, resulting in a significant improvement in cycling stability and mitigation of voltage decay in LRLO/graphite full cells featuring a 3 mAh/cm^2 areal capacity. These findings have the potential to guide the design of surface modification layers for high-voltage cathode materials and inform the utilization of boron-based electrolyte additives in future applications.

Results and Discussion

LBO dry coating optimization and cycling stability improvement

The dry coating method involves physically mixing powder-form LBO precursors with LRLO in the desired weight percentage and calcination of the blended powder. The detailed LRLO sample information is provided in the Material and Method section. The LBO precursors were synthesized through a polyol process, as described in our previous work [14]. The synthesized precursors are organic soft materials featuring boron as a functional group along their C-H backbone (**Figure S1 (a)**). Upon mixing, chemical bonding, such as B-H, O-H, and C-H, is established on the LRLO surface. After calcination, it is anticipated that most of the C-H backbone chains will be removed. However, the presence of boron bonding on the LRLO surface can be confirmed. This is evident as both the stretching and bending modes of B-H bonding, absent in pristine LRLO, become distinctly observable after calcination. The resulting chemical bonding, as illustrated in **Figure S1 (b)**, plays crucial roles in facilitating conformal contact between the precursor and the core material. These attributes emphasize the unique advantages associated with employing polyol precursors for the dry coating process, including enhanced adhesion due to the functional group, as well as flexibility and plasticity. The critical variables for the mixing and calcination step were then optimized, as shown in **Figure S2**. When the mixing time exceeds 20 minutes (**Figure S3 (d)**), secondary particles break apart. Conversely, mixing for less than 5 minutes (**Figure S3 (a)** and **(b)**) reveals agglomeration of LBO precursors. Vigorous mixing for an extended period can impose stress on LRLO, necessitating appropriate mixing conditions. It was determined that mixing for 10 minutes at 1000 rpm induces the most uniform mixing while simultaneously maintaining the secondary particle of LRLO. After blending the powder, calcination is carried out to decompose the organic functional group within the precursor, thereby yielding

the LBO coating layer. As shown in **Figure S2**, optimal conditions for the calcination step are achieved when the surface modification appears uniformly, and LBO precursors are no longer visible. This optimal calcination condition with a dwell temperature of 600 ℃ and a dwell time of 10 hours is further verified through electrochemical evaluations (**Figure S4**).

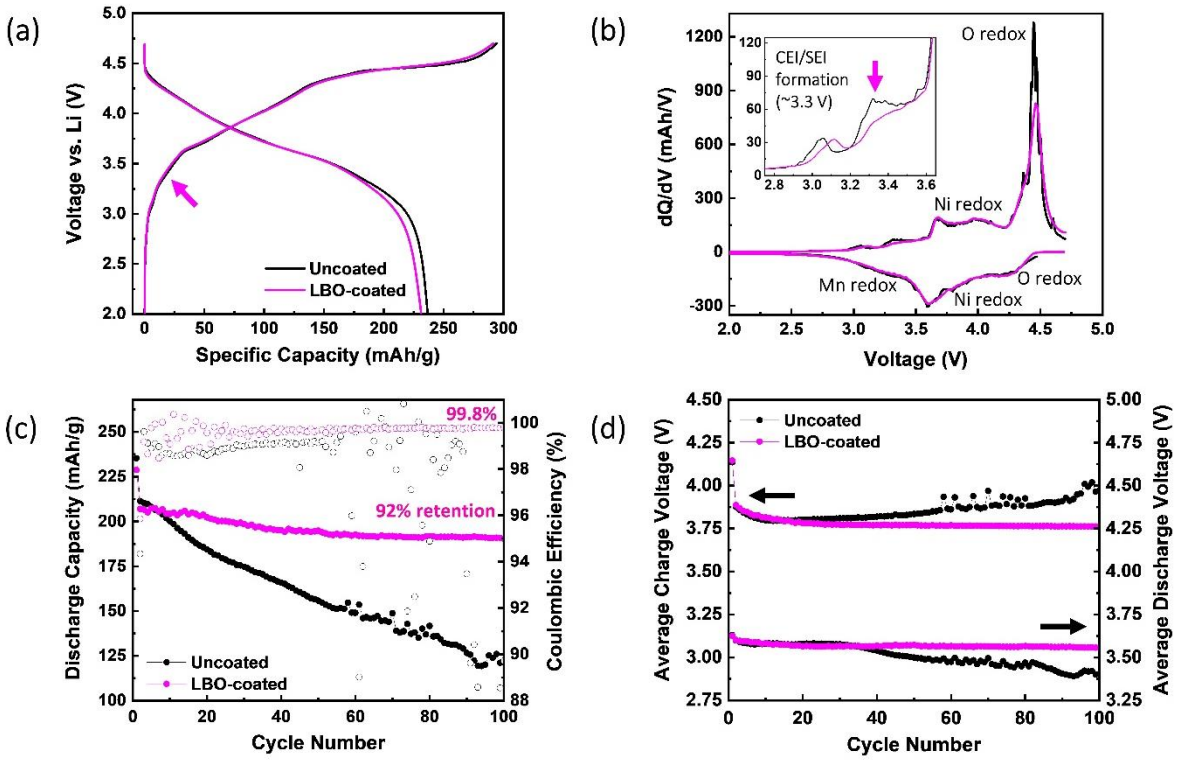

Figure 1. (a) Voltage profiles from uncoated and LBO-coated LRLO/graphite full cell with (b) the corresponding dQ/dV plot. The voltage window of both full cells is 2.0–4.7 V at a current rate of C/20 for the formation cycle (1 C = 270 mAh/g). (c) Full cells cycling performances with (d) the average charge and discharge voltage in the 2.0–4.55 V window at a current rate of C/10.

The LBO-coated LRLO exhibits a similar voltage profile (**Figure 1 (a)**) with little capacity loss compared with the uncoated cathode during the formation cycle in full cell. The dQ/dV plots reveal a lower peak intensity for LBO-coated LRLO in the voltage range associated with electrode/electrolyte interphase formation, around 3.3 V (inset of **Figure 1 (b)**). Uncoated LRLO shows a continuous decrease in capacity from the beginning of the

cycling (**Figure 1 (c)**). In contrast, LBO-coated LRLO demonstrates approximately 92% capacity retention after 100 cycles in full cell. The average charge and discharge voltage plot (**Figure 1 (d)**) substantiates the role of LBO surface modification on LRLO not only in improving capacity retention but also in ameliorating voltage decay.

LBO coating chemistry and durability

The electrochemical assessment confirmed the effect of the surface modification. To further validate these results, an examination of the presence of boron on the cathode surface was conducted. Mixing LRLO and LBO precursors confirms the presence of relatively lighter material on the cathode surface (**Figure S5 (b)**). After calcination, both high-magnification views of the cathode surface (**Figure S5 (c)**) and overall observations at low magnification (**Figure S5 (e)**) did not exhibit evidence of the coating materials. This observation strongly suggests that the surface modification material, LBO, has undergone a reaction with the cathode surface or beyond. Due to LRLO's polycrystalline nature, assessing coating uniformity in SEM-backscattered electrons (BSE) mode posed challenges. In particular, boron chemistry makes it difficult to confirm the coating uniformity using energy dispersive X-ray spectroscopy (EDX) analysis. The boron layer was then distinctly discerned on the cathode surface through STEM-EELS analysis (**Figure 2 (a)**). Elemental mapping verified the partial diffusion of elements toward the cathode subsurface. This observation indicates a modification in the chemical environment between transition metals and boron, suggesting their influence on improving electrochemical performances.

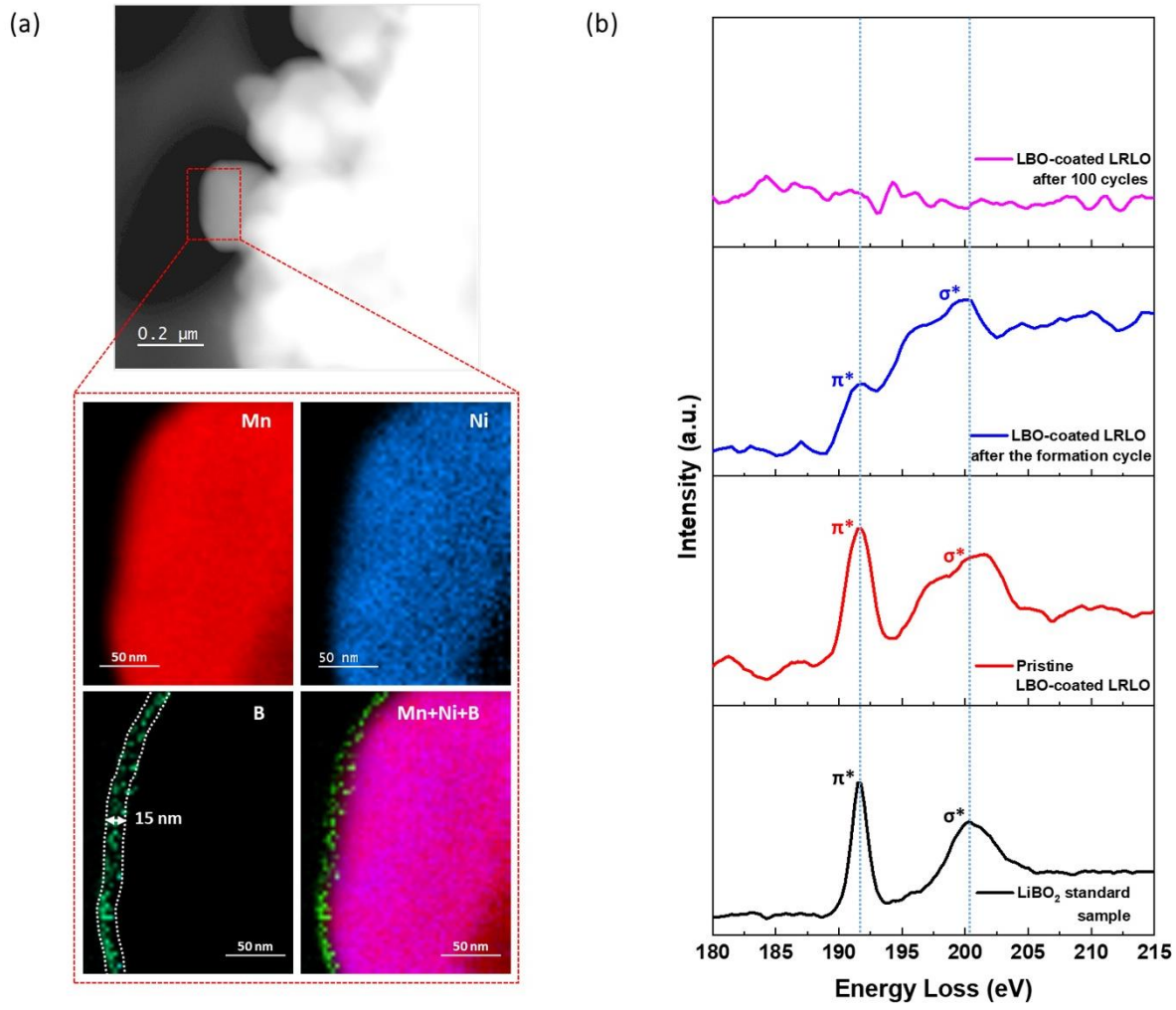

Figure 2. STEM-EELS mapping results of (a) LBO-coated LRLO obtained with the optimal dry coating parameters. (b) STEM-EELS spectra of boron K-edge for examining the changes in LBO under different electrochemical states and $LiBO_2$ standard sample for comparison.

In order to check the durability of the LBO coating layer and understand its chemical environment, STEM-EELS analysis was conducted on the cathode after the first formation cycle in the full cell. The boron coating layer was still present on the cathode surface after the formation cycle (**Figure S6**), albeit in a different chemical environment. **Figure 2 (b)** compares the EELS spectra of the B K-edge from the surface of the LBO-coated cathode before and after electrochemical cycling. The measured near-edge structure for the $LiBO_2$ standard sample is characterized by a sharp peak at 192 eV associated with transitions to

antibonding π* orbitals, and a broad feature at ~ 201 eV originated from σ* orbitals. At the pristine state, the LBO coating layer closely matches the spectrum from the $LiBO_2$ standard sample, while after the formation cycle, the change of the relative peak intensity is observed. Prior literature [25, 26] suggests that the presence of elements such as Ni, Co, and Zn as impurities in boron-based glass can affect the relative peak intensity. Therefore, boron may further diffuse into the transition metal layers during the formation process, which is confirmed through the boron K-edge EELS mapping in **Figure S6**. Following 100 cycles, no boron signal is detected in the boron K-edge spectrum, implying the absence of LBO species on the cathode surface and their reactivity with the electrolyte.

To gain a clear mechanism understanding on the improved full cell performance, tracking boron is essential not only on the cathode but also on the graphite anode. As shown in **Figure 3 (a)**, the presence of a boron layer on the graphite surface with a thickness of up to 15 nm was confirmed after the formation cycle. The layer is thin but uniform and clearly present across the entire surface of the anode, as further confirmed by STEM-EELS spectra analysis (**Figure 3 (b)**). The peak positions and intensity ratios observed on the anode surface were identical to those observed on the cathode surface after the formation cycle. These observations indicate that the boron initially present on the cathode surface migrates through the electrolyte and deposits on the anode surface. This process contributes to the formation of SEI layer, as evidenced by the change in peak intensity around 3.3 V in dQ/dV plots (**Figure 1 (b)**). After 100 cycles, like the cathode surface, there is an absence of any observable boron signal on the graphite anode surface. This reinforces that the LBO species can gradually undergo reactions with the electrolyte during extended cycling periods.

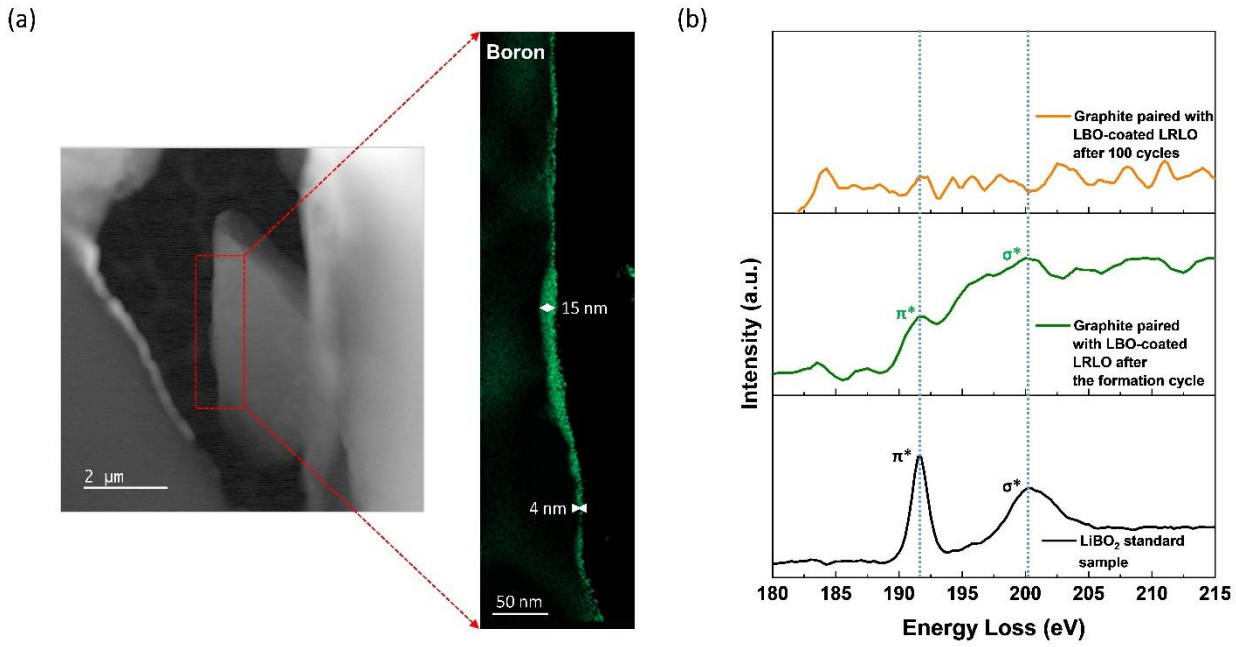

Figure 3. (a) STEM-EELS mapping results of graphite paired with LBO-coated LRLO after the formation cycle in the full cell. (b) EELS spectra of boron K-edge for cycled graphite and $LiBO_2$ standard sample for comparison.

LBO reactivity with electrolyte for performance improvement

The results obtained from STEM-EELS pinpoint the crucial factor of LBO reactivity with electrolyte for the improvement of overall cell performance. Due to insufficient electrolyte amount at the coin cell level, single-layer pouch cells were then assembled for cycling evaluation and electrolyte analysis. The uncoated LRLO pouch cell delivers a capacity retention of 79.9% after 70 cycles at a current rate of C/10. In contrast, the LBO-coated LRLO demonstrates a higher retention of 87.4% with a stabilized discharge capacity from around 40 cycles (**Figure S7 (a)**). Additionally, the charge and discharge voltage plot in **Figure S7 (b)** shows that the uncoated LRLO pouch cell has a voltage hysteresis of 0.37 V, while the LBO-coated LRLO reduces the voltage hysteresis to 0.18 V. To avoid excessive electrolyte consumption with prolonged cycling, the pouch cells were stopped at 70 cycles, at which point a clear difference in gas generation (**Figure S7 (c)**) was observed. The LRLO

pouch cell without LBO coating exhibits evident swelling. This observation underscores the potential of LBO surface modification in reducing the gas generation which arises from the parasitic reactions in the cycled electrolyte at high voltage [27]. Pouch cells of uncoated LRLO and LBO-coated LRLO were disassembled after the formation cycle and after 70 cycles. Centrifuge tubes were utilized to efficiently extract the electrolyte through rotation at 2000 rpm. The extracted electrolyte was then analyzed by ^{19}F-NMR techniques (**Figure S8**).

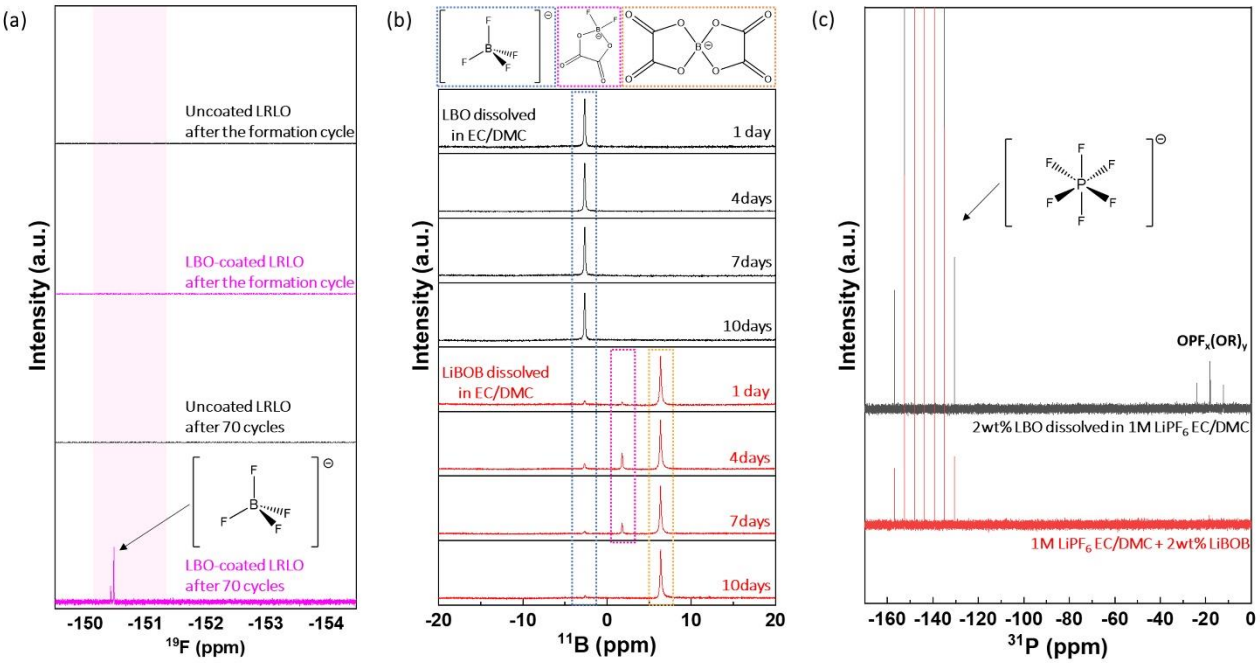

Figure 4. (a) ^{19}F-NMR from different electrolyte samples, including cycled electrolytes from uncoated LRLO and LBO-coated LRLO after the formation cycle and 70 cycles. (b) ^{11}B-NMR and (c) ^{31}P-NMR from different electrolyte samples, including LBO and LiBOB dissolved into carbonate baseline electrolyte.

The presence of BF_4^- anions (**Figure 4 (a)**) is exclusively confirmed in the electrolyte after 70 cycles with LBO-coated LRLO. The formation of BF_4^- is absent even in the initial stage of the LBO-coated LRLO pouch cell, which implies that boron primarily contributes to

forming the CEI/SEI layer during the formation cycle. As cycling progresses, boron progressively dissolves into the electrolyte, leading to the formation of B-F bonding. This observation aligns with STEM-EELS results, revealing the absence of boron on the cathode surface after 100 cycles.

To further investigate the reactivity of LBO, an electrolyte comprising 2 wt% LBO powder dissolved in 1M $LiPF_6$ EC/DMC 3:7 (v%) was examined. For comparison, another electrolyte containing 2 wt% LiBOB additive was also prepared in the same carbonate baseline electrolyte. In our previous study [28], B-F bonding was also present in the cycled electrolyte with LiBOB additive, which comes from the reaction between LiBOB and HF acid generated from electrolyte decomposition. Both electrolytes were stored for 1-, 4-, 7-, and 10-days post-preparation, followed by ^{11}B-NMR analysis to trace boron species (**Figure 4 (b)**). The findings reveal the rapid presence of BF_4^- anions within a day of LBO dissolution. After 10 days, no other boron species, apart from BF_4^-, are detected. This observation implies an immediate reaction of LBO with the fluorine source (PF_6^- anion in the $LiPF_6$ salt) upon dissolution, leading to the formation of B-F bonding. In contrast, when LiBOB is utilized as an electrolyte additive, even after 10 days, a significant portion of the boron persists in the form of BOB^-. The emergence of a small quantity of BF_4^- and $DFOB^-$ in the LiBOB electrolyte after storage is attributed to the disproportionation reaction between fluoride ligands on phosphorus and oxalato ligands on boron (in LiBOB) [29]. The considerably higher reactivity of LBO with the carbonate baseline electrolyte is further confirmed by ^{31}P-NMR analysis (**Figure 4 (c)**). The peak corresponding to PF_6^- in the -160 to -130 ppm range is evident in both electrolytes. However, distinctive peak features around -18 ppm associated with the $OPF_x(OR)_y$ organic compounds are observed solely in the electrolyte containing the LBO additive [30]. These organic compounds arise as byproducts of the reaction between LBO and PF_6^- anions in the electrolyte. The distinction in the reaction pathway leading to the

formation of B-F bonding between LBO and LiBOB additives is crucial in elucidating the mechanism underlying performance improvement, as detailed below.

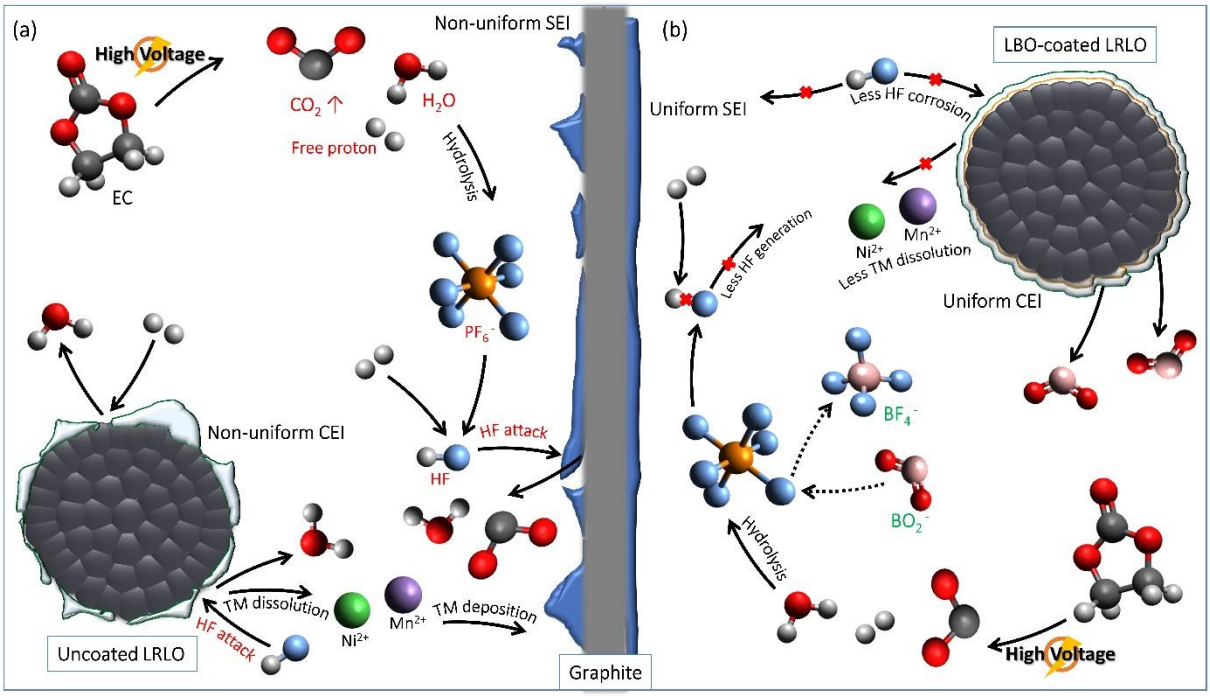

Figure 5. Schematics of performance improvement by LBO-coated LRLO in LRLO/graphite full cell. Reaction pathway for (a) uncoated LRLO/graphite full cell and (b) LBO-coated LRLO/graphite full cell with carbonate baseline electrolyte.

Based on all the above findings, the cycling performance improvement of LBO-coated LRLO in full cell is summarized in **Figure 5**. Cycling under high-voltage, the ethylene carbonate (EC) component of the carbonate-based electrolyte undergoes ring opening process (**Figure 5 (a)**) [31]. Carbonate solvents oxidize and decompose, leading to the release of protons. The liberated protons are highly reactive on the cathode surface, binding with the oxygen and generating H_2O. This H_2O then reacts with $LiPF_6$ salt to form HF acid, which is highly corrosive to the cathode and anode surfaces [32]. On the cathode surface, the attack of HF acid causes the dissolution of transition metal, which subsequently redeposits on the

anode surface through the electrolyte. The inductively coupled plasma mass spectrometry (ICP-MS) soaking test in **Figure S9** reveals a significantly higher concentration of Ni and Mn in the graphite when paired with uncoated LRLO electrode after the formation cycle. The High-angle annular dark-field (HAADF) image (**Figure S10**) of uncoated LRLO is provided for the analysis of the CEI layer after the formation cycle. STEM-EELS mapping reveals distinct clustering of carbon and fluorine, indicating a non-uniform distribution along the surface of primary particles. This observation aligns with the STEM-EDX data presented in **Figure S11**, confirming a similar non-uniform distribution of the SEI layer. Another noteworthy observation is the clear detection of manganese and nickel on the anode surface even after the formation cycle. This indicates that the dissolution and redeposition of transition metals occur even during the formation cycle.

On the other hand, the LBO coating layer on the cathode surface engages in a competitive reaction compared to the $LiPF_6$ hydrolysis process (**Figure 5 (b)**). As confirmed by ^{31}P-NMR, LBO reacts with PF_6^- to form $LiBF_4$ or phosphorus fluorine oxide species. Given that the reaction between $LiPF_6$ and H_2O occurs simultaneously with the competitive interaction involving LBO, the reaction with H_2O is comparatively suppressed, thereby mitigating HF generation. Furthermore, the B-F bonding (613 kJ·mol^{-1}) with much higher bond energy than H-F (565 kJ·mol^{-1}) and P-F (490 kJ·mol^{-1}) signifies that the B-F bond is more thermodynamically stable [28]. Consequently, in contrast to the uncoated LRLO case, LBO-coated LRLO exhibits a more uniform CEI layer with approximately 20 nm in thickness (**Figure S12**), indicating the relative attenuation of severe HF acid attacks during cycling. The STEM-EDX data in **Figure S13** also illustrates a uniform SEI layer, approximately 80 nm thick on the graphite anode paired with LBO-coated LRLO after the formation cycle. Transition metals were also detected in this graphite, highlighting that LBO surface modification cannot completely prohibit the dissolution and redeposition of transition metals.

However, it is crucial to emphasize that the LBO surface modification plays a significant role in mitigating these effects, as indicated by the results from the ICP-MS analysis (**Figure S9**).

The LBO coating cannot prevent the generation of H_2O, which is the intrinsic issue of the EC solvent under highly oxidative environment [33]; however, the continuous production of HF by PF_6^- can be reduced through the competitive reaction between LBO and PF_6^-. In our previous study [28], LiBOB was confirmed to serve as the scavenger for the generated HF acid. In order to completely prevent the HF corrosion to the active materials and their interphase, we explore the synergy effect of employing both approaches: incorporating LBO-coated LRLO as the cathode material and introducing LiBOB as the electrolyte additive.

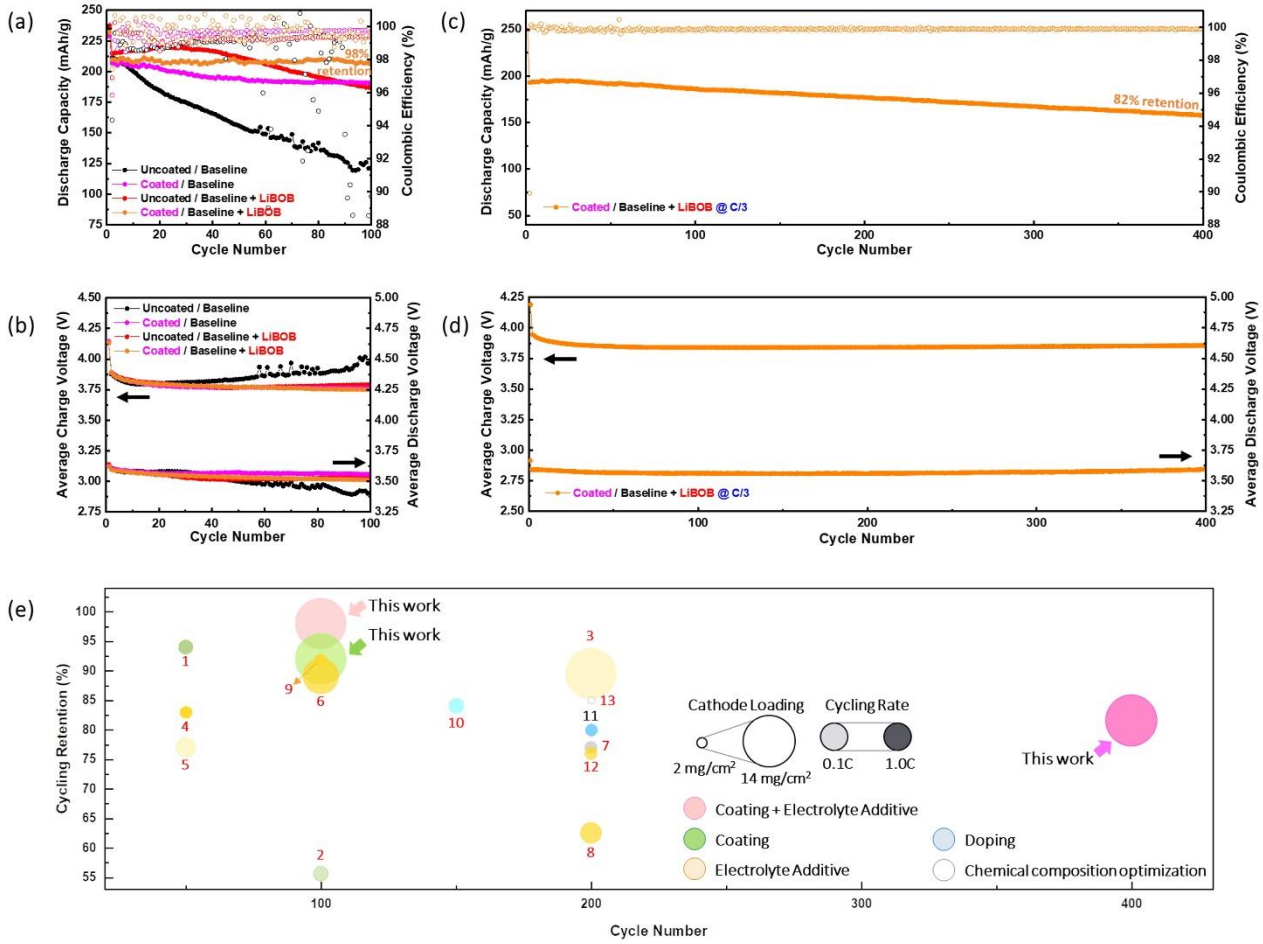

Figure 6. (a) Full cells cycling performance comparison with (b) the corresponding average charge and discharge voltage in the 2.0–4.55 V window at a current rate of C/10. (c) Cycling performance comparison with (d) the corresponding average charge and discharge voltage in the 2.0–4.55 V window at a current rate of C/3. (e) LRLO/graphite full cell performance summary plot. (The numbers refer to the entries in **Table S1** of the Supporting Information. Additionally, red numbers indicate Co-containing LRLO cathode materials, while black numbers indicate Co-free LRLO cathode materials.)

LBO coating and LiBOB additive for long-term cycling stability

Irrespective of the use of electrolyte additives or surface modification, it shows no obvious capacity degradation during the formation cycle (**Figure S14 (a)**). The derivative of the capacity with respect to the cell voltage was then plotted to compare the lithiation/delithiation processes for different cases. Apart from the peak at 3.3 V (corresponding to the CEI/SEI formation), there is no noticeable difference in the dQ/dV vs.

plots (**Figure S14 (b)**). When LiBOB was used as an electrolyte additive or when the surface was modified with LBO, the intensity of the 3.3 V peak in the dQ/dV vs. plots decreases (**Figure S14 (c)**).

To assess the synergy effect, a practical-level long-term cycling was conducted. Under the challenging conditions of high voltage, high loading electrode (3 mAh/cm^2), and a high current rate (C/3), the LBO-coated LRLO/graphite full cell with LiBOB electrolyte additive exhibits excellent performance, with a capacity retention of 82% after 400 cycles (**Figure 6 (c)**). Furthermore, even under high current rate conditions, a minimal voltage decay of 0.019 V was observed for the discharge process up to 400 cycles (**Figure 6 (d)**). Based on the performance summary from the published results of the LRLO/graphite full cell (**Table S1**), our investigation highlights the optimum cycle performance achieved with a Co-free chemical composition and the highest cathode loading (**Figure 6 (e)**). Notably, this synergistic effect persists even under elevated temperatures. The high temperature (45°C) testing results are presented in **Figure S15**. In contrast to the immediate capacity drop of the full cell with uncoated LRLO cathode (black line), LBO surface modification alone exhibits the capacity to endure for approximately 60 cycles (pink line). The inclusion of a 2 wt% LiBOB electrolyte additive extends the cycling capability beyond 200 cycles. This observation underscores the potential to surmount the challenges associated with cycling at elevated temperatures, another obstacle that has impeded the practical application of LRLO, through strategic utilization of boron chemistry.

Conclusions

The oxygen redox products in LRLO, including radical anion complexes, readily engage with carbonate-based electrolytes, causing parasitic side reactions that compromise the

cathode material's lattice structure and result in a rapid deterioration of electrochemical performance. This investigation employs boron chemistry to design a strategy for stabilizing the electrode-electrolyte interphase, proving effective in alleviating capacity and voltage decay. The LBO precursor is synthesized using a polyol process, enabling dry coating on the LRLO surface. Under optimized conditions, a uniform LBO coating layer of 15 nm thickness is achieved, contributing to enhanced cycling stability in LRLO/graphite full cells.

The improved full cell performance is attributed to the surface modification by LBO, which protects LRLO's lattice oxygen, and reacts with PF_6^- anions to suppress HF acid generation. This mechanistic understanding is supported by the observed reduction in transition metal dissolution and mitigated interphase corrosion in LBO-coated LRLO. The further incorporation of LiBOB additive, acting as an HF scavenger, results in promising battery performance for industrial-level applications. The full cell with LBO-coated LRLO cathode demonstrates an impressive 82% capacity retention after 400 cycles at a current rate of C/3, with an average discharge voltage drop of 0.019 V. This minimal voltage decay presents a significant opportunity for engineering LRLO materials towards achieving long-term cycling stability.

Material and methods

Sample preparation: The pristine $Li_{1.222}Ni_{0.349}Mn_{0.651}O_2$ sample (denoted as LRLO) was provided by Umicore. SEM images of the pristine LRLO are presented in **Figure S16 (a-c)**, revealing oval-spherical secondary particles with an average size of approximately 9 μm. The X-ray diffraction (XRD) pattern was obtained for the structural analysis of the pristine LRLO. Rietveld refinement was applied to the collected XRD data to determine the lattice parameters and site occupancies of the pristine LRLO sample, as shown in **Figure S16 (d)**

and **(e)**. The XRD pattern can be matched to the R-3m space group, with lattice parameters a = 2.867(6) Å and c = 14.266(4) Å. The refined occupancies reveal a 6.8% Li/Ni mixing between the Li and TM layers. In summary, the LRLO sample exhibits high material purity and a well-organized layered structure with low Li/Ni mixing, establishing it as a reliable baseline material for this study. For coating material synthesis, 0.03 mol of Polyvinylpyrrolidone (PVP) (MW=50,000) was added to 100 mL of Tetraethylene Glycol (TTEG). We then added 0.015 mol of $LiOH \cdot H_2O$ and 0.015 mol of H_3BO_3 into the solution. After 2 hours of heating the solution at 80 ℃, the products were naturally cooled down, followed by washing in ethanol 7 times. After removing moisture in an 80 ℃ vacuum oven for one day, the dried powder was ground finely using a mortar and pestle, and finally, using a ball mill at 500 rpm for 5 hours with ethanol to make the particle size smaller. The obtained LBO precursor (2% in a weight ratio) was then mixed with the LRLO cathode in a Thinky Mixer (Thinky Corporation) at 2000 rpm for 10 minutes. The well-mixed powder was transferred into the furnace for calcination under different temperatures and dwell time. After calcination, the powder was ground using a mortar and pestle for about 10 minutes.

Electrode preparation: To evaluate the electrochemical performance of LBO-coated LRLO, electrodes using uncoated and LBO-coated LRLO were prepared, with SPC65 (carbon black, TIMCAL Ltd.) as the conductive agent and HSV900 (PVDF, Arkema Inc.) as the binder, in a mass ratio of 80:10:10 and a cathode loading of 3 mAh/cm^2. The mixture was then dissolved in a proper amount of N-methyl-2-pyrrolidone (NMP, ≥ 99%, Sigma-Aldrich) in a Thinky Mixer to form the slurry. The slurry was cast onto Al foil and dried at 80 ℃ in a vacuum oven overnight, followed by 1 hour of drying at elevated temperature of 120 ℃. The cathode was punched into discs with a 12.7 mm diameter and a loading of active mass around 14 mg/cm^2. For LRLO/graphite full cells, both CR2032 and pouch cells were assembled. The graphite electrode used in this work was provided by NIMTE with an active material ratio of

94%. For CR2032 full cells, the graphite electrode was punched into discs with a 13 mm diameter, and the designed N/P ratio was around 1.1. For single layer pouch-type full cells, the cathode size was 44 × 30 mm, and the anode size was 45 × 32 mm. For all the cells, Celgard 2325 was used as the separator. 1M $LiPF_6$ in EC: DMC = 3:7 (vol%) was obtained from Gotion, USA, and is denoted as carbonate baseline electrolyte. All the coin cells were assembled in the Ar-filled glovebox with moisture control (H_2O < 0.5 ppm), and 50 µl of electrolyte was used for each coin cell. The single layer pouch cells were first assembled in the atmosphere without electrolytes. The assembled pouch cells were moved to a heating tray inside the glovebox antechamber and dried at 80 ℃ overnight under vacuum before the electrolyte injection. After drying, the dry pouches were moved inside the Ar-filled glovebox without air exposure, and 500 µl of electrolyte was injected into each cell. The pouch cells with electrolytes were vacuum sealed inside the glovebox and transferred out for further testing.

Electrochemical performance evaluation: After assembling, the coin cell (CR2032) and pouch cell full cells were evaluated by cycling at a rate of C/10 (where 1C is 270 mAh/g) after the formation cycle at a current rate C/20. The electrochemical performances of all the cells were tested either by Neware Battery Test System (Neware Technology Ltd., China) or Arbin BT2000 instruments (Arbin instrument, USA).

Characterizations: FEI Apreo® was applied with 5 kV as the accelerating voltage and 0.1 nA as the beam current for the SEM analysis. We applied a backscattered electron imaging technique to verify the uniformity of the LBO surface modification layer on LRLO, especially for large-area coating uniformity evaluation. The microscope detector was first changed to T1 mode, which was extremely sensitive to backscattered electrons. Then, the accelerated voltage was lowered to detect the surface information. The contrast gradually

appeared when lowering the accelerated voltage from 5 kV to 200 V, while the optimized voltage was 500 V to 1000 V to acquire clear images. A Thermofisher Talos F200X G2 transmission electron microscope, equipped with a Ceta camera and operated at 200 kV, was used to acquire STEM-EELS and STEM-EDX data. To minimize possible electron beam irradiation effects, EELS spectra presented in this work were acquired from areas without pre-beam irradiation. ICP-MS analysis was performed with a Thermo iCAP RQ ICP-MS to analyze the elemental concentration in fresh and cycled electrolytes. The ^{11}B, ^{19}F, and ^{31}P-NMR measurements of the electrolyte samples were performed with a JEOL ECA 500 spectrometer. Liquid NMR samples were prepared by adding 10 μL of electrolyte to 600 μL of DMSO-D6 solution, and 50 μl of α, α, α-Trifluorotoluene was added to each sample as the reference and sealed in an NMR tube inside the Ar-filled glovebox for further measurement. The NMR spectrums were analyzed with MestReNova. All spectra were calibrated with α, α, α-Trifluorotoluene at −63.72 ppm. FT-IR spectra were collected using Nicolet 6700 Fourier transform infrared spectrometer. Approximately 5−10 mg of LRLO was dried at 80 ℃ for at least 12 h before the FT-IR analysis.

Author contributions

N. P., M. Z., and Y. S. M. conceived the idea. N. P. and M. Z. designed the experiments. N. P. synthesized the organic nano-sized boron precursor and performed LBO-coating on LRLO cathode material. N. P. collected and analyzed the data for SEM, ICP-MS, liquid NMR, FT-IR, and electrochemical performances. B. H. collected and processed the data for STEM-EELS and STEM-EDX. All authors discussed the results and contributed to the manuscript. All authors have approved the final version of the manuscript.

Conflicts of interest

The authors declare no competing financial interest.

Acknowledgements

This work was supported by Umicore. STEM-EELS in this work were performed at the Nano3 of UCSD, a member of the National Nanotechnology Coordinated Infrastructure, which is supported by the National Science Foundation (Grant ECCS-1542148). The ICP-MS was conducted at the Environmental and Complex Analysis Laboratory (ECAL) in the Chemistry and Biochemistry department at UC San Diego. The NMR in this work was conducted at the Chemistry NMR facility at UC San Diego. The authors are grateful for Umicore providing the LRLO cathode materials used in the research. The authors thank Prof. Zhaoping Liu's group from Ningbo Institute of Materials Technology & Engineering (NIMTE) for providing the graphite anode.

References

[1] Armand, M., Axmann, P., Bresser, D., Copley, M., Edström, K., Ekberg, C., Guyomard, D., Lestriez, B., Novák, P., Petranikova, M., Porcher, W., Trabesinger, S., Wohlfahrt-Mehrens, M., & Zhang, H. (2020). Lithium-ion batteries – Current state of the art and anticipated developments. *Journal of Power Sources*, *479*. https://doi.org/10.1016/j.jpowsour.2020.228708

[2] Radin, M. D., Hy, S., Sina, M., Fang, C., Liu, H., Vinckeviciute, J., Zhang, M., Whittingham, M. S., Meng, Y. S., & van der Ven, A. (2017). Narrowing the Gap between Theoretical and Practical Capacities in Li-Ion Layered Oxide Cathode Materials. In *Advanced Energy Materials* (Vol. 7, Issue 20). Wiley-VCH Verlag. https://doi.org/10.1002/aenm.201602888

[3] Wu, F., Kim, G. T., Diemant, T., Kuenzel, M., Schür, A. R., Gao, X., Qin, B., Alwast, D., Jusys, Z., Behm, R. J., Geiger, D., Kaiser, U., & Passerini, S. (2020). Reducing Capacity and Voltage Decay of Co-Free $Li_{1.2}Ni_{0.2}Mn_{0.6}O_2$ as Positive Electrode Material for Lithium Batteries Employing an Ionic Liquid-Based Electrolyte. *Advanced Energy Materials*, *10*(34). https://doi.org/10.1002/aenm.202001830

[4] Zhang, B., Wang, L., Wang, X., Zhou, S., Fu, A., Yan, Y., Wang, Q., Xie, Q., Peng, D., Qiao, Y., & Sun, S. G. (2022). Sustained releasing superoxo scavenger for tailoring the electrode-electrolyte interface on Li-rich cathode. *Energy Storage Materials*, *53*, 492–504. https://doi.org/10.1016/j.ensm.2022.09.032

[5] Zhang, M., Liu, H., Liu, Z., Fang, C., & Meng, Y. S. (2018). Modified Coprecipitation Synthesis of Mesostructure-Controlled Li-Rich Layered Oxides for Minimizing Voltage Degradation. *ACS Applied Energy Materials*, *1*(7), 3369–3376. https://doi.org/10.1021/acsaem.8b00545

[6] Heng, Y.-L., Gu, Z.-Y., Guo, J.-Z., Yang, X.-T., Zhao, X.-X., & Wu, X.-L. (2022). Research progress on the surface/interface modification of high-voltage lithium oxide cathode materials. *Energy Materials*, *2*(3). https://doi.org/10.20517/energymater.2022.18

[7] Zhang, M., Kitchaev, D. A., Lebens-Higgins, Z., Vinckeviciute, J., Zuba, M., Reeves, P. J., Grey, C. P., Whittingham, M. S., Piper, L. F. J., van der Ven, A., & Meng, Y. S. (2022). Pushing the limit of 3d transition metal-based layered oxides that use both cation and anion redox for energy storage. In *Nature Reviews Materials* (Vol. 7, Issue 7, pp. 522–540). Nature Research. https://doi.org/10.1038/s41578-022-00416-1

[8] Singer, A., Zhang, M., Hy, S., Cela, D., Fang, C., Wynn, T. A., Qiu, B., Xia, Y., Liu, Z., Ulvestad, A., Hua, N., Wingert, J., Liu, H., Sprung, M., Zozulya, A. v., Maxey, E., Harder, R., Meng, Y. S., & Shpyrko, O. G. (2018). Nucleation of dislocations and their dynamics in layered oxide cathode materials during battery charging. *Nature Energy*, *3*(8), 641–647. https://doi.org/10.1038/s41560-018-0184-2

[9] Li, Y., Zuba, M. J., Bai, S., Lebens-Higgins, Z. W., Qiu, B., Park, S., Liu, Z., Zhang, M., Piper, L. F. J., & Meng, Y. S. (2021). Regeneration of degraded Li-rich layered

oxide materials through heat treatment-induced transition metal reordering. *Energy Storage Materials*, *35*, 99–107. https://doi.org/10.1016/j.ensm.2020.11.013

[10] Hy, S., Liu, H., Zhang, M., Qian, D., Hwang, B. J., & Meng, Y. S. (2016). Performance and design considerations for lithium excess layered oxide positive electrode materials for lithium ion batteries. In *Energy and Environmental Science* (Vol. 9, Issue 6, pp. 1931–1954). Royal Society of Chemistry. https://doi.org/10.1039/c5ee03573b

[11] Zhao, T., Chen, S., Chen, R., Li, L., Zhang, X., Xie, M., & Wu, F. (2014). The positive roles of integrated layered-spinel structures combined with nanocoating in low-cost Li-rich cathode $Li[Li_{0.2}Fe_{0.1}Ni_{0.15}Mn_{0.55}]O_2$ for lithium-ion batteries. *ACS Applied Materials and Interfaces*, *6*(23), 21711–21720. https://doi.org/10.1021/am506934j

[12] Zhang, X., Belharouak, I., Li, L., Lei, Y., Elam, J. W., Nie, A., Chen, X., Yassar, R. S., & Axelbaum, R. L. (2013). Structural and electrochemical study of Al_2O_3 and TiO_2 Coated $Li_{1.2}Ni_{0.13}Mn_{0.54}Co_{0.13}O_2$ cathode material using ALD. *Advanced Energy Materials*, *3*(10), 1299–1307. https://doi.org/10.1002/aenm.201300269

[13] Kim, S. Y., Park, C. S., Hosseini, S., Lampert, J., Kim, Y. J., & Nazar, L. F. (2021). Inhibiting Oxygen Release from Li-rich, Mn-rich Layered Oxides at the Surface with a Solution Processable Oxygen Scavenger Polymer. *Advanced Energy Materials*, *11*(30). https://doi.org/10.1002/aenm.202100552

[14] Park, N. R., Li, Y., Yao, W., Zhang, M., Han, B., Mejia, C., Sayahpour, B., Shimizu, R., Bhamwala, B., Dang, B., Kumakura, S., Li, W., & Meng, Y. S. (2023). Understanding the Role of Lithium Borate as the Surface Coating on High Voltage Single Crystal $LiNi_{0.5}Mn_{1.5}O_4$. *Advanced Functional Materials*. https://doi.org/10.1002/adfm.202312091

[15] Zheng, J., Gu, M., Xiao, J., Polzin, B. J., Yan, P., Chen, X., Wang, C., & Zhang, J. G. (2014). Functioning mechanism of AlF_3 coating on the Li- and Mn-rich cathode materials. *Chemistry of Materials*, *26*(22), 6320–6327. https://doi.org/10.1021/cm502071h

[16] Wu, F., Zhang, X., Zhao, T., Li, L., Xie, M., & Chen, R. (2015). Multifunctional $ALPO_4$ coating for improving electrochemical properties of low-cost $Li[Li_{0.2}Fe_{0.1}Ni_{0.15}Mn_{0.55}]O_2$ cathode materials for lithium-ion batteries. *ACS Applied Materials and Interfaces*, *7*(6), 3773–3781. https://doi.org/10.1021/am508579r

[17] Shi, S. J., Tu, J. P., Tang, Y. Y., Zhang, Y. Q., Liu, X. Y., Wang, X. L., & Gu, C. D. (2013). Enhanced electrochemical performance of LiF-modified $LiNi_{1/3}Co_{1/3}Mn_{1/3}O_2$ cathode materials for Li-ion batteries. *Journal of Power Sources*, *225*, 338–346. https://doi.org/10.1016/j.jpowsour.2012.10.065

[18] Jo, C. H., Cho, D. H., Noh, H. J., Yashiro, H., Sun, Y. K., & Myung, S. T. (2015). An effective method to reduce residual lithium compounds on Ni-rich $Li[Ni_{0.6}Co_{0.2}Mn_{0.2}]O_2$ active material using a phosphoric acid derived Li_3PO_4

nanolayer. *Nano Research*, *8*(5), 1464–1479. https://doi.org/10.1007/s12274-014-0631-8

[19] Jiang, J., Li, Y., Liu, J., Huang, X., Yuan, C., & Lou, X. W. (2012). Recent advances in metal oxide-based electrode architecture design for electrochemical energy storage. In *Advanced Materials* (Vol. 24, Issue 38, pp. 5166–5180). https://doi.org/10.1002/adma.201202146

[20] Wang, W., Yin, Z., Wang, J., Wang, Z., Li, X., & Guo, H. (2015). Effect of heat-treatment on Li_2ZrO_3-coated $LiNi_{1/3}Co_{1/3}Mn_{1/3}O_2$ and its high voltage electrochemical performance. *Journal of Alloys and Compounds*, *651*, 737–743. https://doi.org/10.1016/j.jallcom.2015.08.114

[21] Zhou, L., Yin, Z., Tian, H., Ding, Z., Li, X., Wang, Z., & Guo, H. (2018). Spinel-embedded and Li_3PO_4 modified $Li[Li_{0.2}Mn_{0.54}Ni_{0.13}Co_{0.13}]O_2$ cathode materials for High-Performance Li-Ion battries. *Applied Surface Science*, *456*, 763–770. https://doi.org/10.1016/j.apsusc.2018.06.114

[22] Liu, W., Oh, P., Liu, X., Myeong, S., Cho, W., & Cho, J. (2015). Countering Voltage Decay and Capacity Fading of Lithium-Rich Cathode Material at 60 °Cby Hybrid Surface Protection Layers. *Advanced Energy Materials*, *5*(13). https://doi.org/10.1002/aenm.201500274

[23] Zhou, L. J., Yin, Z. L., Ding, Z. Y., Li, X. H., Wang, Z. X., & Guo, H. J. (2018). CeO_2 coating to improve the performance of $Li[Li_{0.2}Mn_{0.54}Ni_{0.13}Co_{0.13}]O_2$. *Ionics*, *24*(9), 2533–2542. https://doi.org/10.1007/s11581-017-2387-0

[24] Liu, H., Qian, D., Verde, M. G., Zhang, M., Baggetto, L., An, K., Chen, Y., Carroll, K. J., Lau, D., Chi, M., Veith, G. M., & Meng, Y. S. (2015). Understanding the Role of NH_4F and Al_2O_3 Surface Co-modification on Lithium-Excess Layered Oxide $Li_{1.2}Ni_{0.2}Mn_{0.6}O_2$. *ACS Applied Materials and Interfaces*, *7*(34), 19189–19200. https://doi.org/10.1021/acsami.5b04932

[25] Sauer, H., Brydson, R., Rowley, P. N., Engel, W., & Thomas, J. M. (1993). Determination of coordinations and coordination-specific site occupancies by electron energy-loss spectroscopy: an investigation of boron-oxygen compounds Dedicated to Professor Elmar Zeitler on the occasion of his 65th birthday. In *Ultramicroscopy* (Vol. 49).

[26] Lelong, G., Cormier, L., Hennet, L., Michel, F., Rueff, J. P., Ablett, J. M., & Monaco, G. (2017). Lithium borate crystals and glasses: How similar are they? A non-resonant inelastic X-ray scattering study around the B and O K-edges. *Journal of Non-Crystalline Solids*, *472*, 1–8. https://doi.org/10.1016/j.jnoncrysol.2017.06.012

[27] Yao, W., Chouchane, M., Li, W., Bai, S., Liu, Z., Li, L., Chen, A. X., Sayahpour, B., Shimizu, R., Raghavendran, G., Schroeder, M. A., Chen, Y. T., Tan, D. H. S., Sreenarayanan, B., Waters, C. K., Sichler, A., Gould, B., Kountz, D. J., Lipomi, D. J., Zhang, M., & Meng, Y. S. (2023). A 5 V-class cobalt-free battery cathode with high

loading enabled by dry coating. *Energy and Environmental Science*, *16*(4), 1620–1630. https://doi.org/10.1039/d2ee03840d

[28] Li, Y., Li, W., Shimizu, R., Cheng, D., Nguyen, H. N., Paulsen, J., Kumakura, S., Zhang, M., & Meng, Y. S. (2022). Elucidating the Effect of Borate Additive in High-Voltage Electrolyte for Li-Rich Layered Oxide Materials. *Advanced Energy Materials*, *12*(11). https://doi.org/10.1002/aenm.202103033

[29] Xiao, A., Yang, L., & Lucht, B. L. (2007). Thermal reactions of $LiPF_6$ with added LiBOB. *Electrochemical and Solid-State Letters*, *10*(11), 241–244. https://doi.org/10.1149/1.2772084

[30] Dong, Y., Demeaux, J., Zhang, Y., Xu, M., Zhou, L., MacIntosh, A. D., & Lucht, B. L. (2017). Improving the Performance at Elevated Temperature of High Voltage Graphite/$LiNi_{0.5}Mn_{1.5}O_4$ Cells with Added Lithium Catechol Dimethyl Borate. *Journal of The Electrochemical Society*, *164*(2), A128–A136. https://doi.org/10.1149/2.0331702jes

[31] Metzger, M., Strehle, B., Solchenbach, S., & Gasteiger, H. A. (2016). Hydrolysis of Ethylene Carbonate with Water and Hydroxide under Battery Operating Conditions. *Journal of The Electrochemical Society*, *163*(7), A1219–A1225. https://doi.org/10.1149/2.0411607jes

[32] Li, W., Cheng, D., Shimizu, R., Li, Y., Yao, W., Raghavendran, G., Zhang, M., & Meng, Y. S. (2022). Artificial cathode electrolyte interphase for improving high voltage cycling stability of thick electrode with Co-free 5 V spinel oxides. *Energy Storage Materials*, *49*, 77–84. https://doi.org/10.1016/j.ensm.2022.04.002

[33] Liu, M., Vatamanu, J., Chen, X., Xing, L., Xu, K., & Li, W. (2021). Hydrolysis of $LiPF_6$-Containing Electrolyte at High Voltage. *ACS Energy Letters*, *6*(6), 2096–2102. https://doi.org/10.1021/acsenergylett.1c00707